

Source localization using particle filtering on FPGA for robotic navigation with imprecise binary measurement

Adithya Krishna, André van Schaik, *Fellow, IEEE*, and Chetan Singh Thakur, *Senior Member, IEEE*

Abstract—Particle filtering is a recursive Bayesian estimation technique that has gained popularity recently for tracking and localization applications. It uses Monte Carlo simulation and has proven to be a very reliable technique to model non-Gaussian and non-linear elements of physical systems. Particle filters outperform various other traditional filters like Kalman filters in non-Gaussian and non-linear settings due to their non-analytical and non-parametric nature. However, a significant drawback of particle filters is their computational complexity, which inhibits their use in real-time applications with conventional CPU or DSP based implementation schemes. This paper proposes a modification to the existing particle filter algorithm and presents a high-speed and dedicated hardware architecture. The architecture incorporates pipelining and parallelization in the design to reduce execution time considerably. The design is validated for a source localization problem wherein we estimate the position of a source in real-time using the particle filter algorithm implemented on hardware. The validation setup relies on an Unmanned Ground Vehicle (UGV) with a photodiode housing on top to sense and localize a light source. We have prototyped the design using Artix-7 field-programmable gate array (FPGA), and resource utilization for the proposed system is presented. Further, we show the execution time and estimation accuracy of the high-speed architecture and observe a significant reduction in computational time. Our implementation of particle filters on FPGA is scalable and modular, with a low execution time of about $5.62 \mu\text{s}$ for processing 1024 particles and can be deployed for real-time applications.

Keywords—Particle filters, Field programmable gate array, Bearings-only tracking, Bayesian filtering, Unmanned ground vehicle, Hardware architectures, Real-time processing.

I. INTRODUCTION

Emergency response operations such as disaster relief and military applications often require localization of a contaminant chemical or biological source in an unknown environment. Unmanned vehicles are gaining popularity in such applications in recent times due to reduced human involvement and ability to carry out the task remotely. These autonomous systems can eventually supplement human intervention in various safety-critical and hazardous missions. Nevertheless, conditions in which these missions are conducted vary drastically depending on the environmental factors, that result in the sensor receiving noise-corrupted measurements. This poses a

significant challenge to the unmanned vehicles to navigate and locate a target in an unknown environment autonomously.

In our study, we demonstrate autonomous source localization using a UGV (robot) utilizing the Bearings-only tracking (BOT) model [1] for light source localization with noise-corrupted input measurements as a proof-of-concept. The BOT model utilized here uses a particle filter algorithm [2] to increase the robustness to false detections, and noise-corrupted measurements. In recent times, there is growing popularity of particle filters (PFs) in signal processing and communication applications to solve various state estimation problems like tracking [3], localization, navigation [4], and fault diagnosis [5]. PFs have been applied to achieve filtering for models described using a dynamic state-space approach comprising a system model describing the state evolution and a measurement model describing the noisy measurements of the state [6]. In most real-time scenarios, these models are non-linear and non-Gaussian. Traditional filters like Kalman filters prove to be less reliable for such applications, and it has been shown that PFs outperform conventional filters in such scenarios [7].

PFs are inherently Bayesian in nature, intending to construct a posterior density of the state (e.g., location of a target or source) from observed noisy measurements. In PFs, posterior of the state is represented by a set of weighted random samples known as particles. A weighted average of the samples gives the state estimate (location of the source). PFs use three major steps: Sampling, Importance, and Re-sampling for state estimation, thus deriving the name SIR filter. In the sampling step, particles from the prior distribution are drawn. The importance step is used to update the weights of particles based on input measurements. The re-sampling step prevents any weight degeneracy by discarding particles with lower weights and replicating particles having higher weights. Since PFs apply a recursive Bayesian calculation, all particles must be processed for sampling, importance, and re-sampling steps. Then, the process is repeated for the next input measurement, resulting in enormous computational complexity. Further, execution time of PFs is proportional to the number of particles, which inhibits the use of PFs in various real-time applications wherein a large number of particles need to be processed to obtain a good performance. Various implementation strategies (discussed below) have been suggested in the literature to alleviate this problem and make the PFs feasible in real-time applications.

A. Krishna and C. S. Thakur are with the Department of Electronic Systems Engineering, Indian Institute of Science, Bangalore - 560012, India (Email: {adithyaik,esthakur}@iisc.ac.in); A. van Schaik is with the International Centre for Neuromorphic Systems, The MARCS Institute, Western Sydney University, Australia. (Email: A.VanSchaik@westernsydney.edu.au);

A. State-of-the-art

The first hardware prototype for PFs was proposed by Athalye et al. [8] by implementing a standard SIR filter on an FPGA. They provided a generic hardware framework for realizing SIR filters and implemented traditional PFs without parallelization on FPGA. As an extension to [8], Bolic et al. [9] suggested a theoretical framework for parallelizing the re-sampling step by proposing distributed algorithms called Re-sampling with Proportional Allocation (RPA) and Re-sampling with Non-proportional Allocation (RNA) of particles to minimize execution time. The design complexity of RPA is significantly higher than that of RNA due to non-deterministic routing and complex routing protocol. Though the RNA solution is preferred over RPA for high-speed implementations with low design time, the RNA algorithm trades performance for speed improvement. Miao et al. [10] proposed a parallel implementation scheme for PFs using multiple processing elements (PEs) to reduce execution time. However, the communication overhead between the PEs increases linearly with the number of PEs, making the architecture not scalable to process a large number of particles. Agrawal et al. [11] proposed an FPGA implementation of a PF algorithm for object tracking in video. Ye and Zhang [12] implemented an SIR filter on the Xilinx Virtex-5 FPGA for bearings-only tracking applications. Sileshi et al. [13]–[15] suggested two methods for implementation of PFs on an FPGA: the first method is a hardware/software co-design approach for implementing PFs using MicroBlaze soft-core processor, and the second approach is a full hardware design to reduce execution time. Velmurugan [16] proposed an FPGA implementation of a PF algorithm for tracking applications without any parallelization using the Xilinx system generator tool.

Further, several real-time software-based implementation schemes have been proposed with an intent to reduce computational time. Hendeby et al. [17] proposed the first Graphical Processing Unit (GPU) based PFs and showed that a GPU-based implementation outperforms a CPU implementation in terms of processing speed. Murray et al. [18] provided an analysis of two alternative schemes for the re-sampling step based on Metropolis and Rejection samplers to reduce the overall execution time. They compared it with a standard Systematic resamplers [19] over GPU and CPU platforms. Chitchian et al. [20] devised an algorithm for implementing a distributed computation PF on GPU for fast real-time control applications. Zhang et al. [21] proposed an architecture for implementing PFs on a DSP efficiently for tracking applications in wireless networks. However, these software-based methods have their own drawbacks when it comes to hardware implementation owing to their high computational complexity. Therefore, it is essential to develop a high-speed and dedicated hardware design with the capacity to process a large number of particles in a specified time to meet the speed demands of real-time applications. This paper addresses this issue by proposing a high-speed architecture that is massively parallel and easily scalable to handle a large number of particles. The benefits of the proposed architecture are explained in the following subsection.

B. Our contributions

The contributions of this paper are on the algorithmic and hardware fronts:

1) *Algorithmic Contribution:* We present an experimental framework and a measurement model to solve the source localization problem using the bearing-only tracking model in real-time. In our experiment, we employ a light source as the target/source to be localized and a UGV carrying an array of photodiodes to sense and localize the source. The photodiode measurements and the UGV position are processed to estimate the bearing of the light source relative to the UGV. Based on the bearing of the light source, we try to localize the source using the PF algorithm. Reflective objects and other stray light sources are also picked by the sensor (photodiodes), leading to false detections. In this study, we have successfully demonstrated that our PF system is robust to noise and can localize the source even when the environment is noisy. However, the PFs are computationally very expensive, and the execution time often becomes unrealistic using a traditional CPU based platform. The primary issue faced during the design of high-speed PF architecture is the parallelization of the re-sampling step. The re-sampling step is inherently not parallelizable as it needs the information of all particles. To overcome this problem, we propose a modification to the standard SIR filter (cf. Algorithm 1) to make a parallel and high-speed implementation possible. The modified algorithm proposed (cf. Algorithm 2) uses a network of smaller filters termed as sub-filters, each doing the processing independently and concurrently. The processing of total N particles is partitioned into K sub-filters so that at most N/K particles are processed within a sub-filter. This method reduces the overall computation time by a factor of K . The modified algorithm also introduces an additional particle routing step (cf. Algorithm 2), which distributes the particles among the sub-filters and makes the parallel implementation of re-sampling possible. The particle routing step is integrated with the sampling step in the architecture proposed and does not require any additional time for computation. We also compare the estimation accuracy of the standard algorithm with the modified algorithm in Section VII-C and conclude that there is no significant difference in estimation error between the modified and the standard approach. Additionally, the modified algorithm achieves a very low execution time of about $5.62 \mu\text{s}$ when implemented on FPGA, compared to 64 ms on Intel Core i7-7700 CPU with eight cores clocking at 3.60 GHz for processing 1024 particles and outperforms other state-of-the-art FPGA implementation techniques.

2) *Hardware Contribution:* We implemented the proposed modified SIR algorithm on an FPGA, and key features of the architecture are:

- **Modularity:** We divide the overall computation into multiple sub-filters, which process a fixed number of particles in parallel, and the processing of the particles is local to the sub-filter. This modular approach makes the design simple and adaptable as it allows us to customize the number of sub-filters in the design depending on the sampling rate of the input measurement and the amount of parallelism

needed.

- Scalability: Our architecture can be scaled easily to process a large number of particles without increasing the execution time, by using additional sub-filters.
- Design complexity: The proposed architecture relies on the exchange of particles between sub-filters. However, communication and design complexity increase proportionally with the number of sub-filters used in the design. In our architecture, we employ a simple ring topology to exchange particles between sub-filters to reduce complexity and design time.
- Memory utilization: The sampling step uses particles from the previous time instant to compute the particles of the current time instant. This requires the sampled and re-sampled particles to be stored in two separate memories. The straightforward implementation of the modified SIR algorithm needs $2 \times K$ memory elements each of depth M for storing the sampled and re-sampled particles for K sub-filters. Here, M is the number of particles in a sub-filter ($M = N/K$). However, applications involving non-linear models require a large number of particles [22]. This would make the total memory requirement $2 \times K$ significant for large K or M . The proposed architecture reduces this memory requirement to K memory elements each of depth M using a dual-port ram, as explained in Section VI-A1. Therefore, the proposed architecture reduces memory utilization and is more energy-efficient due to reduced memory accesses.
- Real-time: Since all sub-filters operate in parallel, the execution time is significantly reduced compared to that of other traditional implementation schemes that use just one filter block [8]. Our implementation has a very low execution time of about $5.62 \mu\text{s}$ (i.e., a sampling rate of 178 kHz) for processing 1024 particles and outperforms other state-of-the-art implementations, thus making it possible to be deployed in real-time scenarios.
- Flexibility: The proposed architecture is not limited to a single application, and the design can be easily modified by making slight changes to the architecture for other PF applications.

The architecture was successfully implemented on an Artix-7 FPGA. Our experimental results demonstrate the effectiveness of the proposed architecture for source localization using the PF algorithm with noise-corrupted input measurements.

The rest of the paper is organized as follows: We provide the theory behind Bayesian filtering and PFs in Section II and III, respectively. The experimental setup for source localization using a Bearings-only tracking (BOT) model is presented in section IV. In this model, input to the filter is a time-varying angle (bearing) of the source, and each input is processed by the PF algorithm implemented on hardware to estimate the source location. Further, in section V, we propose algorithmic modifications to the existing PF algorithm that make the high-speed implementation possible. The architecture for implementing PFs on hardware is provided in Section VI. Evaluation of resource utilization on the Artix-7 FPGA, performance analysis in terms of execution time, estimation accuracy, and the experimental results are provided in Section VII.

II. BAYESIAN FRAMEWORK

In a dynamic state space model, the evolution of the state sequence x_t is defined by:

$$x_t = f_t(x_{t-1}, w_t) \quad (1)$$

where, f_t is a nonlinear function of the state x_{t-1} , and w_t represents the process noise. The objective is to recursively estimate the state x_t based on a measurement defined by:

$$z_t = g_t(x_t, v_t) \quad (2)$$

where, g_t is a nonlinear function describing the measurement model, and z_t is the observation vector of the system corrupted by measurement noise v_t at time instant t .

From a Bayesian standpoint, the objective is to construct the posterior $p(x_t|z_{1:t})$ of the state x_t from the measurement data $z_{1:t}$ up to time t . By definition, constructing the posterior is done in two stages namely, prediction and update.

The prediction stage involves using the system model (cf. Eq. 1) to obtain a prediction probability density function (PDF) of the state at time instant t , using the Chapman-Kolmogorov equation:

$$p(x_t|z_{1:t-1}) = \sum_{x_{t-1}} p(x_t|x_{t-1})p(x_{t-1}|z_{1:t-1}) \quad (3)$$

where, the transition probability $p(x_t|x_{t-1})$ is defined by system model (cf. Eq. 1).

In the update stage, the measurement data z_t at time step t is used to update the PDF obtained from the prediction stage using Bayes rule, to construct the posterior:

$$p(x_t|z_{1:t}) = \frac{p(z_t|x_t)p(x_t|z_{1:t-1})}{\sum_{x_t} p(z_t|x_t)p(x_t|z_{1:t-1})} \quad (4)$$

where, $p(z_t|x_t)$ is a likelihood function defined by the measurement model (cf. Eq. 2).

The process of prediction (cf. Eq. 3) and update (cf. Eq. 4) are done recursively for every new measurement z_t . Constructing the posterior based on Bayes rule is a conceptual solution and is analytically estimated using traditional Kalman filters. However, in a non-Gaussian and non-linear setting, the analytic solution is intractable, and approximation-based methods such as PFs are employed to find an approximate Bayesian solution. A detailed illustration of the Bayesian framework and its implementation for estimating the state of a system is provided by Thakur et al. [23].

III. PARTICLE FILTERS BACKGROUND

The key idea of PFs is to represent the required posterior density by a set of random samples termed as particles, with associated weights, and to compute the state estimate based on these particles and weights. The particles and their associated weights are denoted by $\{x_t^i, w_t^i\}_{i=1}^N$, where N is the total number of particles. x_t^i denotes the i^{th} particle at time instant t . w_t^i represents the weight corresponding to the particle x_t^i . The most commonly used PF named the sampling, importance, and re-sampling filter (SIRF) is presented in Algorithm 1.

In the sampling step, particles are drawn from the prior density $p(x_t|x_{t-1}^i)$ to generate particles at time instant t .

Algorithm 1 : SIR Algorithm

Initialization: Set the particle weights of previous time step to $1/N$, $\{w_{t-1}^i\}_{i=1}^N = 1/N$.

Input: Particles from previous time step $\{x_{t-1}^i\}_{i=1}^N$ and measurement z_t .

Output: Particles of current time step $\{\hat{x}_t^i\}_{i=1}^N$.

Method:

- 1: **Sampling and Importance:**
 - 2: for $i = 1$ to N do
 - 3: Sample $x_t^i \sim p(x_t|x_{t-1}^i)$
 - 4: Calculate $w_t^i = w_{t-1}^i p(z_t|x_t^i)$
 - 5: end for
 - 6: **Re-sampling:** Deduce the re-sampled particles $\{\hat{x}_t^i\}_{i=1}^N$ from $\{x_t^i, w_t^i\}_{i=1}^N$.
-

$p(x_t|x_{t-1}^i)$ is deduced from (1). Intuitively, it can be thought as propagating the particles from time step $t-1$ to t . The sampled set of particles at time instant t is denoted by $\{x_t^i\}_{i=1}^N$. At time instant 0, particles are initialized with prior distribution to start the iteration. These particles are then propagated in time successively.

The importance step assigns weights to every particle x_t^i based on the measurement z_t . By definition, the weights are given by:

$$w_t^i = w_{t-1}^i p(z_t|x_t^i) \quad (5)$$

However, weights of the previous time step are initialized to $1/N$ i.e $w_{t-1}^i = 1/N$. Thus, we have:

$$w_t^i \propto p(z_t|x_t^i) \quad (6)$$

The re-sampling step is used to deal with the degeneracy problem in PFs. In the re-sampling step, particles with lower weights are eliminated, and particles with higher weights are replicated to compensate for the discarded particles depending on the weight w_t^i associated with the particle x_t^i . The re-sampled set of particles is denoted by $\{\hat{x}_t^i\}_{i=1}^N$.

IV. BEARINGS-ONLY TRACKING MODEL

This section briefly describes an experimental setup and a measurement model to solve the Bearings-Only Tracking (BOT) problem using the PF algorithm. As a real-world application, we consider a source localization problem wherein we try to estimate the source position based on the received sensor measurements in a noisy environment.

A. Overview of the experimental setup

In our experiment, an omnidirectional light source serves as a source to be localized. A photodiode housing mounted on top of a UGV (cf. Fig. 1(a)) constitutes a sensor to measure the relative intensity of light in a horizontal plane. The space around the UGV is divided into 8 sectors with 45° angular separation, as shown in Fig. 1(b), and an array of 8 photodiodes are placed inside the circular housing to sense the light source in all directions. The housing confines the angle of exposure of the photodiode to 45° . Depending on the light

incident on each photodiode, we consider the output of the photodiode to be either 0 or 1.

The PF algorithm applied to the BOT model requires dynamic motion between the sensor and source [24]. We consider a stationary source, and a moving sensor mounted on a UGV, in our experimental setup. The UGV is made to traverse in the direction of the source and eventually converges to the source. Reflective sources and other stray light sources are potential sources of noise picked up by the sensor, producing false detections. A target-originated measurement, along with noise, is sensed by the photodiodes and processed in addition to the UGV position data, to estimate a bearing of the light source relative to the UGV. Based on the bearing of the light source, we try to estimate its position using the PF algorithm.

B. Measurement model

The position of UGV (x_t^{UGV}) at time instant t is defined by the Cartesian co-ordinate system:

$$x_t^{UGV} = [X_t^{UGV}, Y_t^{UGV}]$$

The orientation of the longitudinal axis of UGV is represented by ϕ_t^{UGV} which gives its true bearing.

The source is considered to be stationary, and its co-ordinates in the 2-dimensional setting is given by:

$$x_t = [X_t, Y_t] \quad (7)$$

At time instant t , a set of 8 photodiode measurements are captured $z_t = \{z_t^1, z_t^2 \dots z_t^8\}$, which comprise of the target-associated measurement and clutter noise. Then, based on the measurement model (2), the source-associated measurement can be modelled as:

$$z_t = g(x_t) + v_t \quad (8)$$

Since the measurement gives the bearing information of the source, we have:

$$g(x_t) = \tan^{-1} \left(\frac{Y_t - Y_t^{UGV}}{X_t - X_t^{UGV}} \right) \quad (9)$$

The four-quadrant inverse tangent function evaluated from $[0, 2\pi)$ gives the true bearing of the source.

The relevant probabilities needed to model the sensor imperfections and clutter noise are as follows:

- (i) The probability of clutter noise (n_t) produced by a stray or reflective light source is: $p(n_t) = \beta$.
- (ii) The probability of the j^{th} photodiode output being 1 i.e., ($z_t^j = 1$) either due to light source or clutter noise is: $p(z_t^j|x_t, n_t) = \alpha$.
- (iii) If there is a light source in the sector j , then j^{th} photodiode output will be 1 with a probability of α irrespective of noise. The likelihood of photodiode output being 1 or 0 in the presence of the source is:

$$p(z_t^j|x_t) = \begin{cases} \alpha, & \text{for } z_t^j = 1. \\ 1 - \alpha, & \text{for } z_t^j = 0. \end{cases} \quad (10)$$

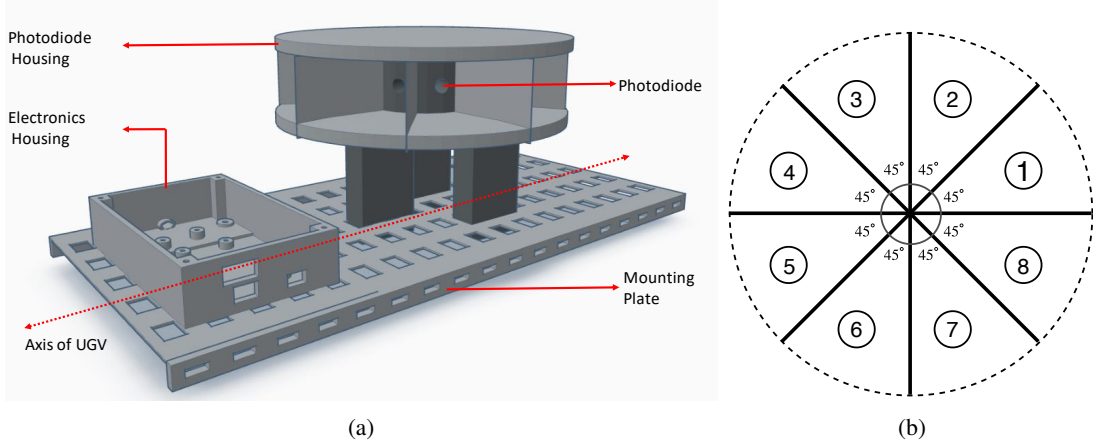


Fig. 1: UGV Design. (a) Schematic of the UGV with a photodiode housing mounted on top. (b) The region around the UGV is divided into 8 sectors with 45° angular separation.

- (iv) If there is no source in sector j , then there is a noise source with probability β . The likelihood of photodiode output being 1 or 0 in the absence of source is:

$$p(z_t^j | \tilde{x}_t) = \begin{cases} \alpha\beta, & \text{for } z_t^j = 1. \\ 1 - \alpha\beta, & \text{for } z_t^j = 0. \end{cases} \quad (11)$$

These two likelihoods are used in our system to model the sensor imperfections and noise, and even with high noise probability β , the PF algorithm is robust enough to localize the source.

V. ALGORITHMIC MODIFICATION OF SIRF FOR REALIZING HIGH-SPEED ARCHITECTURE

In this section, we suggest modifications to the standard SIR algorithm to make it parallelizable. The key idea of the high-speed architecture is to utilize multiple parallel filters, termed as sub-filters, working simultaneously, and performing sampling, importance and re-sampling operations independently on particles. The architecture utilizes K sub-filters in parallel to process a total of N particles. Thus, the number of particles processed within each sub-filter is $M = N/K$. In this way, the number of particles processed within each sub-filter is reduced by a factor K , compared to conventional filters.

The sampling and importance steps are inherently parallelizable since there is no data dependency for particle generation and weight calculation. However, the re-sampling step cannot be parallelized as it needs to have the information of all particles. This creates a major bottleneck in the parallel implementation scheme. Thus, in addition to the SIR stage, we introduce a particle routing step, as shown in Algorithm 2, to route particles between sub-filters. The particle routing step enables the distribution of particles among sub-filters, and the re-sampling step can be effectively parallelized.

The particles and their associated weights in sub-filter k at time step t are represented by $\{x_t^{(k,i)}, w_t^{(k,i)}\}_{i=1}^M$, for $k = 1, \dots, K$. The particle $x_t^{(k,i)}$ represents the position in the Cartesian co-ordinate system.

Algorithm 2 : High-level description of each sub-filter k performing SIR and particle routing operations.

Initialization: Set the particle weights of previous time step to $1/M$, $\{w_{t-1}^{(k,i)}\}_{i=1}^M = 1/M$.

Input: Particles from previous time step $\{x_{t-1}^{(k,i)}\}_{i=1}^M$ and measurement z_t

Output: Particles of current time step $\{\hat{x}_t^{(k,i)}\}_{i=1}^M$

Method:

- 1: **Particle Routing:** Exchange Q particles with neighbouring sub-filters.
 - 2: $\{x_{t-1}^{(k,q)}\}_{q=1}^Q \leftarrow \{x_{t-1}^{(k-1,q)}\}_{q=1}^Q$ for $k = 2, \dots, K$, and
 - 3: $\{x_{t-1}^{(k,q)}\}_{q=1}^Q \leftarrow \{x_{t-1}^{(K,q)}\}_{q=1}^Q$ for $k=1$.
 - 4: **Sampling and Importance:**
 - 5: for $i = 1$ to M do
 - 6: Sample $x_t^{(k,i)} \sim p(x_t | x_{t-1}^{(k,i)})$
 - 7: Calculate $w_t^{(k,i)} = w_{t-1}^{(k,i)} p(z_t | x_t^{(k,i)})$
 - 8: end for
 - 9: **Re-sampling:** Compute the re-sampled particles $\{\hat{x}_t^{(k,i)}\}_{i=1}^M$ from $\{x_t^{(k,i)}, w_t^{(k,i)}\}_{i=1}^M$.
-

VI. ARCHITECTURE OVERVIEW

In this section, we present a high-speed architecture for PFs, based on the modified SIRF algorithm presented in Section V.

The top-level architecture shown in Fig. 2 utilizes a filter bank consisting of K sub-filters working in parallel. Sampling, importance, and re-sampling operations are carried out within a sub-filter. In addition to the SIR step, a fixed number of particles are routed between sub-filters after the completion of every iteration as part of a particle routing operation. The sub-filters are connected based on ring-topology inside the filter bank. M particles are time-multiplexed and processed within each sub-filter, and $Q = M/2$ particles are exchanged with neighbouring sub-filters. Since the number of particles exchanged and the routing topology are fixed, the proposed architecture has very low design complexity. The design can

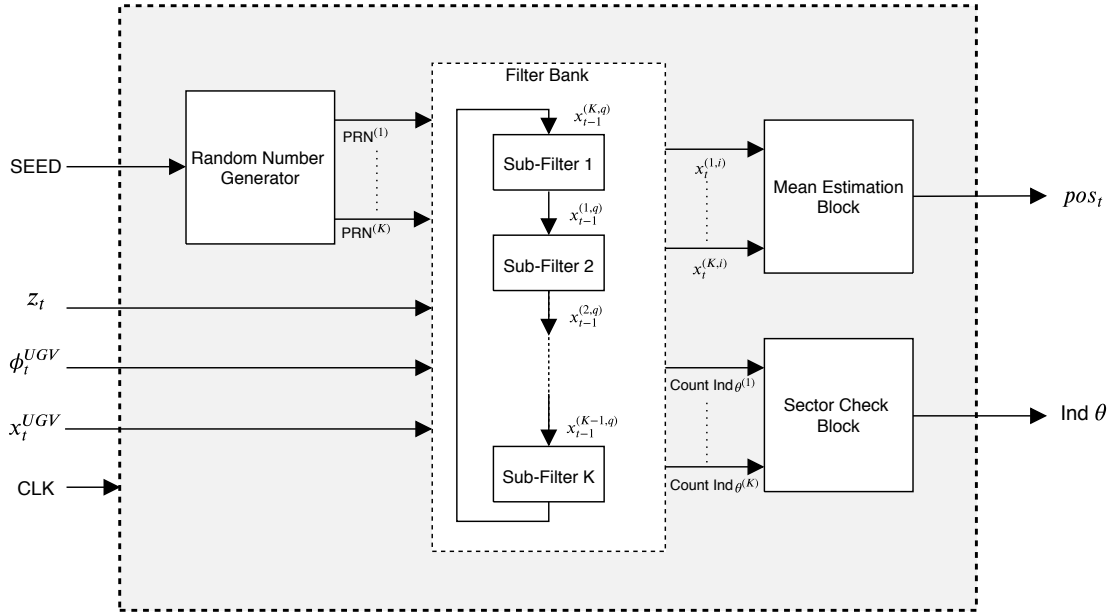


Fig. 2: Top-level architecture of the realized particle filter algorithm.

be easily scaled up to process a large number of particles (N) by replicating sub-filters. The binary measurements of the eight photodiodes (z_t) are fed as an input to the filter bank along with the true bearing (ϕ_t^{UGV}) and the position of the UGV (x_t^{UGV}). Random number generation needed for the sampling and re-sampling steps is provided by a random number generator block. We use a parallel multiple output LFSR architecture presented by Milovanović et al. [25] for random number generation. As our internal variables are 16 bits in size, a 16 bit LFSR is used. Further, a detailed description of the sub-filter architecture is provided in Section VI-A. The sector check block, described in Section VI-B, computes the particle population in each of the eight sectors and outputs a sector index that has the maximum particle population. This information is used by the UGV to traverse in the direction of the source. The mean computational block used to calculate the global mean of all N particles from K sub-filters to estimate the source location (pos_t), is explained in Section VI-C.

A. Sub-filter architecture

The sub-filter is the main computational block responsible for particle generation, processing, and filtering. It consists of three main sub-modules, namely, sampling, importance and re-sampling, as shown in Fig. 3. The sampling and importance blocks are pipelined in operation. The re-sampling step cannot be pipelined with the former steps as it requires weight information of all particles. Thus, it is started after the completion of the importance step. Since sampling and importance stages are pipelined, together they take M clock cycles to iterate for M particles, as shown in Algorithm 2 from line 5 to line 8. The particle routing between the sub-filters is done along with the sampling step and does not require any additional cycles. The re-sampling step takes $3M$ clock cycles, as discussed in Section VI-A3.

1) *Sampling and routing*: The sampling step involves generating new sampled particles $\{x_t^{(k,i)}\}_{i=1}^M$ by propagating the re-sampled particles $\{\hat{x}_{t-1}^{(k,i)}\}_{i=1}^M$ from the previous time step using the dynamic state space model:

$$x_t^{(k,i)} \sim p(x_t | \hat{x}_{t-1}^{(k,i)}) \quad (12)$$

Conventionally, particles $\{x_t^{(k,i)}\}_{i=1}^M$ are used to generate the weights $\{w_t^{(k,i)}\}_{i=1}^M$ in the importance unit, and using these weights we determine the re-sampled particles $\{\hat{x}_t^{(k,i)}\}_{i=1}^M$. Further, $\{\hat{x}_t^{(k,i)}\}_{i=1}^M$ is utilized to obtain particles $\{x_{t+1}^{(k,i)}\}_{i=1}^M$ of the next time step. Thus, with the straightforward approach, we would need two memories each of depth M to store $\{x_t^{(k,i)}\}_{i=1}^M$ and $\{\hat{x}_t^{(k,i)}\}_{i=1}^M$ within a sub-filter. Similarly, for K sub-filters we would require $2 \times K$ memory elements, each of depth M . This increases memory usage for higher K or M . In this paper, we propose a novel scheme to store the particles using a single dual-port memory instead of two memory blocks, which brings down the total memory requirement for storing particles to K memory elements, each of depth M .

In this scheme, since the re-sampled particles are actually the subset of sampled particles (i.e., $\{\hat{x}_t^{(k,i)}\}_{i=1}^M \subset \{x_t^{(k,i)}\}_{i=1}^M$) instead of storing $\{\hat{x}_t^{(k,i)}\}_{i=1}^M$ in a different memory, we can use the same memory as $\{x_t^{(k,i)}\}_{i=1}^M$ and use suitable pointers or indices to read $\{\hat{x}_t^{(k,i)}\}_{i=1}^M$.

The re-sampling unit in our case is modified such that instead of returning re-sampled particles $\hat{x}_{t-1}^{(k,i)}$, it returns the indices of replicated ($\text{Ind } R^{(k,i)}$) and discarded ($\text{Ind } D^{(k,i)}$) particles (cf. Fig. 3). $\text{Ind } R^{(k,i)}$ is used as a read address of the dual-port particle memory shown in Fig. 4 to point to the re-sampled particles $\hat{x}_{t-1}^{(k,i)}$. The dual-port memory enables us to perform read and write operations simultaneously; however, this might result in data overwriting. For example, consider six particles, after re-sampling particle 2 ($x_{t-1}^{(k,2)}$) is replicated four times; particle 5 ($x_{t-1}^{(k,5)}$) is replicated two times and

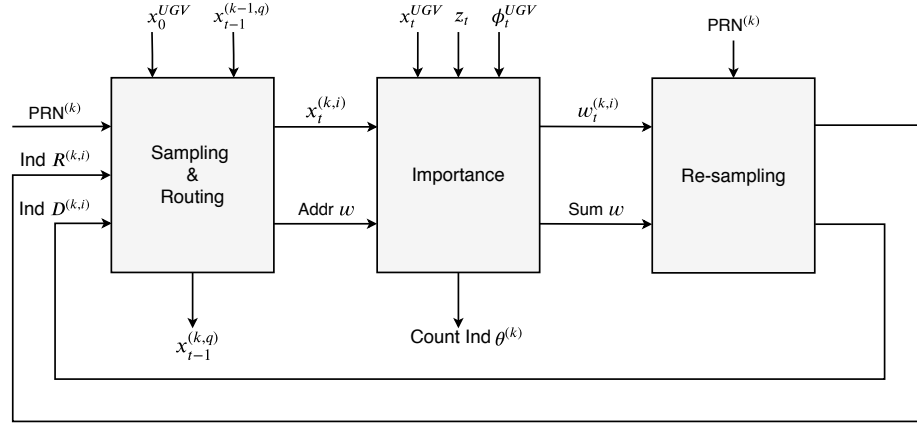


Fig. 3: Sub-filter architecture.

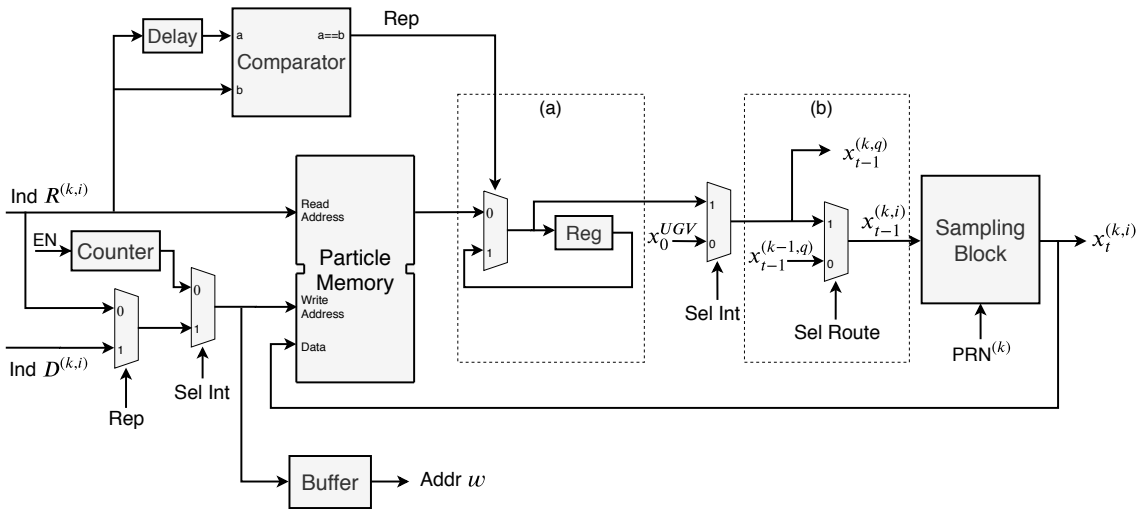


Fig. 4: Sampling and routing unit architecture.

particles 1, 3, 4 & 6 are discarded. The re-sampling unit returns $\text{Ind } R = (2, 2, 2, 2, 5, 5)$ and $\text{Ind } D = (1, 3, 4, 6)$. The read sequence of the dual-port memory is $(2, 2, 2, 2, 5 \& 5)$ and the write sequence is $(2, 1, 3, 4, 5 \& 6)$. Initially, particle 2 ($x_{t-1}^{(k,2)}$) is read from the dual-port memory and after propagation in the sampling block, the sampled particle $x_t^{(k,i)}$ is written back to the memory location 2. Next, particle 2 is read again from memory location 2. However, this time the content of the location is changed and it no longer holds the original particle $x_{t-1}^{(k,2)}$, which causes an error while reading. In order to avoid this scenario, we introduce a sub-block (a) (cf. Fig. 4), wherein when we read the particle from the memory for the first time, it is temporarily stored in a register. Hence, whenever there is a replication in $\text{Ind } R$ or read address, we read the particle from the register instead of memory. The Rep signal is generated by comparing $\text{Ind } R$ with its previous value and if both are same, Rep will be made high.

Further, we introduce a sub-block (b) (cf. Fig. 4), which is responsible for routing the particles between neighbouring sub-filters. Out of M particles read from the particle memory of sub-filter k , the first $M/2$ particles, i.e., $\{x_{t-1}^{(k,q)}\}_{q=1}^{M/2}$ are

Algorithm 3 : Sampling block pseudocode

Input: Particles from previous time step $x_{t-1}^{(k,i)} = [X_{t-1}^{(k,i)}, Y_{t-1}^{(k,i)}]$ and random number $PRN^{(k)} = [PRN_x^{(k)}, PRN_y^{(k)}]$.

Output: Particles of current time step $x_t^{(k,i)}$.

Method:

- 1: for $i = 1$ to M do
 - 2: $X_t^{(k,i)} = X_{t-1}^{(k,i)} + PRN_x^{(k)} * std$
 - 3: $Y_t^{(k,i)} = Y_{t-1}^{(k,i)} + PRN_y^{(k)} * std$ $\triangleright std$ is the standard deviation.
 - 4: $x_t^{(k,i)} = [X_t^{(k,i)}, Y_t^{(k,i)}]$
 - 5: end for
-

sent to sub-filter $k + 1$, and simultaneously the first $M/2$ particles, i.e., $\{x_{t-1}^{(k-1,q)}\}_{q=1}^{M/2}$, of sub-filter $k - 1$ are read and fed to the sampling block of sub-filter k . The sampling block propagates the particles from time step $t - 1$ to time step t . The routed particles from sub-filter $k - 1$ $\{x_{t-1}^{(k-1,q)}\}_{q=1}^{M/2}$, and last $M/2$ local particles $\{x_{t-1}^{(k,q)}\}_{q=M/2+1}^M$ read from particle

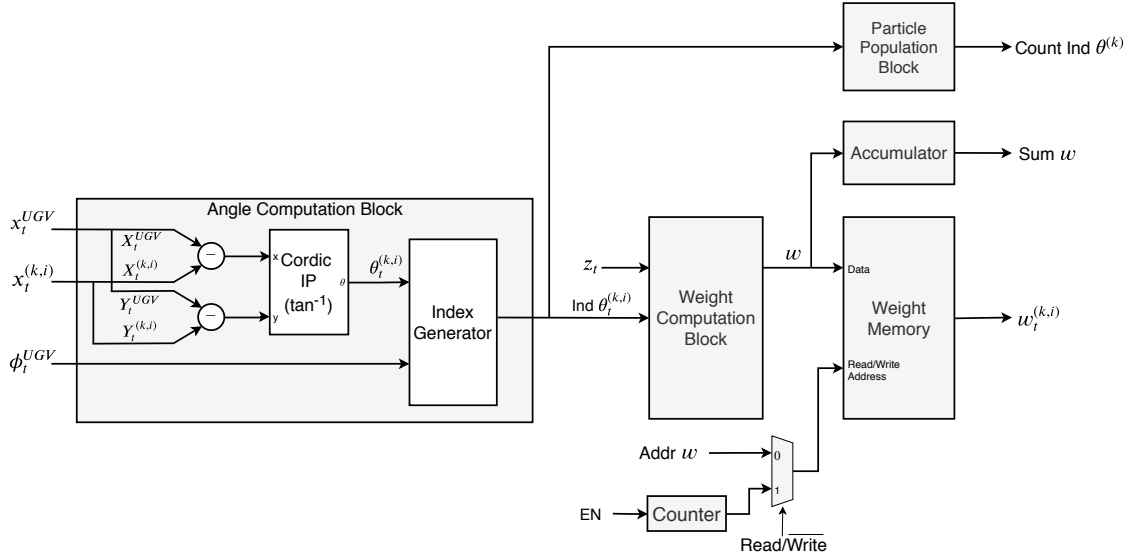


Fig. 5: Importance unit architecture.

memory of sub-filter k are propagated by the sampling block and written back to the memory. The input to the sampling block are particles of time step $t-1$ ($x_{t-1}^{(k,i)}$) and the output are particles of current time step t ($x_t^{(k,i)}$). The sampling block pseudocode is provided by Algorithm 3. The random number $PRN^{(K)}$ needed for random sampling of particles as shown in Algorithm 3, line 2 and line 3 is provided by a random number generator block (cf. Fig. 2). The *Sel Route* signal is used to control the switching between the local and routed particles by making it low for the first $M/2$ cycles and then making it high for the next $M/2$ cycles. Further, at time instant 0, we feed the UGV position x_0^{UGV} as a prior to the sampling block to distribute the particles around the UGV. The *Sel Int* control signal is made low in the first iteration, i.e., at time instant 0, and then made high for the subsequent iterations.

2) *Importance*: The importance unit computes the weights of the particles based on the photodiode measurements z_t given by:

$$w_t^{(k,i)} = w_{t-1}^{(k,i)} p(z_t | x_t^{(k,i)}) \quad (13)$$

$w_{t-1}^{(k,i)}$ is initialized to $1/M$. Estimation of $p(z_t | x_t^{(k,i)})$ involves determining the angle of each particle ($\theta_t^{(k,i)}$), which is computed using an inverse tangent function based on the position of UGV (x_t^{UGV}) and position of the particle ($x_t^{(k,i)}$), as follows:

$$\theta_t^{(k,i)} = \tan^{-1} \left(\frac{Y_t^{(k,i)} - Y_t^{UGV}}{X_t^{(k,i)} - X_t^{UGV}} \right)$$

where, $X_t^{(k,i)}$ and $Y_t^{(k,i)}$ represents the co-ordinates of the particle $x_t^{(k,i)}$ in two-dimensional Cartesian co-ordinate system.

The inverse tangent function is implemented using a Cordic IP block provided by Xilinx [26]. The architecture of the importance unit is shown in Fig. 5. The index generator block estimates the angle of the particles with respect to the

longitudinal axis of the UGV based on the bearing of the UGV (ϕ_t^{UGV}). In addition to this, the index generator block is used for determining the sector indices ($\text{Ind } \theta_t^{(k,i)}$) of the particles based on the angle information. The sector indices of the particle can be defined as follows:

$$\text{Ind } \theta_t^{(k,i)} = \lceil 4/\pi * (\theta_t^{(k,i)} - \phi_t^{UGV}) \rceil$$

z_t is 8 bit wide data consisting of 8 binary photodiode measurements $\{z_t^1, z_t^2 \dots z_t^8\}$. Based on the measurement z_t and the sector indices of the particles, weights are generated by the weight computation block. These weights are stored in the weight memory using the address provided by the sampling unit, to store weights in the same order as the sampled particles $x_t^{(k,i)}$. The sum of all the weights required by the re-sampling unit is obtained by an accumulator. The particle population block is used to estimate the number of particles present in each of the eight sectors, using the sector indices of the particles for a given sub-filter. The particle count in each of the eight sectors of sub-filter k is concatenated and given as the output $\text{Count Ind } \theta^{(k)}$. For example, if sector 1 has 15 particles, sector 3 has 14 particles, and sector 5 has 3 particles, then $\text{Count Ind } \theta^{(k)} = \{15, 0, 14, 0, 3, 0, 0, 0\}$.

3) *Re-sampling*: The re-sampling step replicates particles with higher weights and discards particles with lower weights. This is accomplished by utilizing a Systematic re-sampling algorithm shown in Algorithm 4. A detailed description of the systematic re-sampling algorithm is provided in [8], [19]. The weights and sum of all weights are obtained from the importance unit. The random number (U_0) needed to compute the parameter U_scale in line 2 of Algorithm 4 is provided by the Random number generator block shown in Fig. 2. The algorithm presented works with un-normalized weights, which will avoid M division operations on all particles to implement normalization. The division required to compute A_w in line 1 of Algorithm 4 is implemented using the right shift operation. This approach consumes fewer resources

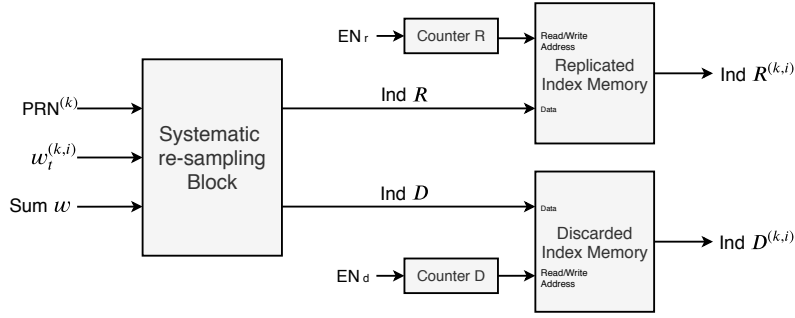


Fig. 6: Re-sampling unit architecture.

and area on hardware. The replicated and discarded indices generated by the systematic re-sampling block are stored in their respective memories, as shown in Fig. 6. In the worst-case scenario, the inner loop of Algorithm 4 takes $2M$ cycles for execution in hardware as it involves fetching M weights from weight memory and doing M comparison operations. Further, line 13 and line 14 take M cycles to obtain M replicated indices. Thus, in total, the execution of the re-sampling step requires $2M + M = 3M$ cycles.

Algorithm 4 : Systematic Re-sampling.

Input: Un-normalized weights ($\{w_t^{(k,i)}\}_{i=1}^M$) of M particles, summation of all the weights in a sub-filter (Sum w) and the uniform random number (U_0) between $[0, 1]$

Output: Replicated index (Ind R) and Discarded index (Ind D).

Method:

- 1: Compute $A_w = \frac{Sum w}{M}$
 - 2: Initialize : $U_scale = U_0 \times A_w$
 - 3: $s = 0, p = 0, m = 0$
 - 4: **for** $i=1$ to M **do**
 - 5: **while** $s < U_scale$ **do**
 - 6: $p = p + 1$
 - 7: $s = s + w^{(k,p)}$
 - 8: **if** $s < U_scale$ **then**
 - 9: $m = m + 1$
 - 10: Ind $D^{(k,m)} = p$
 - 11: **end if**
 - 12: **end while**
 - 13: $U_scale = U_scale + A_w$
 - 14: Ind $R^{(k,i)} = p$
 - 15: **end for**
-

B. Sector check block

The direction/orientation of the UGV is decided by the population of particles in different sectors and is used to move towards the source. This is achieved by the sector check block, which estimates the particle population in each of the eight sectors and gives the sector index with maximum particle count. The block diagram shown in Fig. 7 utilizes eight parallel adders to count the number of particles in each sector. The particle count in a given sector of K sub-filters is fed as an

input to the adder. Count Ind $\theta_n^{(k)}$ in Fig. 7 denotes the particle count in sector n of sub-filter k . The output of an adder gives the total particle population in a particular sector. Furthermore, the sector index (Ind θ) having maximum particle count is estimated using a max computation block. The UGV uses this information to traverse in the direction of the source.

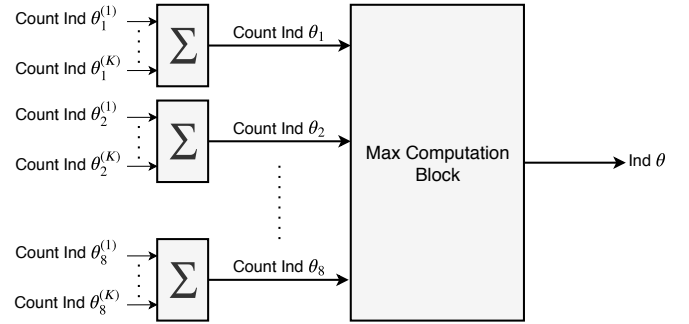


Fig. 7: Sector check block architecture.

C. Mean estimation block

The mean of total N particle positions is estimated using the mean estimation block. Particle positions from K sub-filters are fed in parallel and accumulated over M cycles to generate the sum, which is further divided by N , by right shifting $\log_2(N)$ times to get the mean. In our implementation, we consider N as a power of 2. The mean gives an estimate of the position of the source pos_t .

VII. RESULTS

In this section, we present resource utilization of the proposed design on an FPGA. We also evaluate the execution time of the proposed architecture as a function of number of sub-filters and inspect the estimation accuracy by scaling the number of particles. We then compare our design with state-of-the-art implementations. Furthermore, we present experimental results for the source localization problem implemented on an FPGA using the proposed architecture.

A. Resource utilization

The architecture presented was implemented on an Artix-7 FPGA. Resource utilization of the implemented design

TABLE I: Resource utilization on Artix-7 FPGA.

Sub-filters K	Occupied slices	Slice LUTs	LUTRAM	Slice Registers	Block RAM
1	505 (1.5%)	1,437 (1.07%)	51 (0.11%)	1,735 (0.65%)	2 (0.55%)
2	942 (2.8%)	2,847 (2.13%)	102 (0.22%)	3,259 (1.22%)	4 (1.10%)
4	1,710 (5.1%)	5,494 (4.11%)	204 (0.44%)	6,297 (2.35%)	8 (2.19%)
8	3,465 (10.3%)	10,973 (8.20%)	408 (0.88%)	12,356 (4.62%)	16 (4.38%)
16	6,834 (20.3%)	21,885 (16.36%)	816 (1.77%)	24,460 (9.14%)	32 (8.77%)
32	14,513 (43.1%)	43,804 (32.74%)	1,632 (3.53%)	48,645 (18.18%)	64 (17.53%)
64	29,290 (87%)	86,101 (64.35%)	3,264 (7.06%)	95,570 (35.71%)	128 (35.07%)

for different number of sub-filters is summarized in Table I. The number of particles per sub-filter (M) was fixed to 32 for synthesizing the design. All memory modules shown in the architecture for storing particles, weights, replicated, and discarded indices are mapped into embedded 18kb block random access memory (BRAM) available on the FPGA, using a Block Memory Generator (BMG) IP [27] provided by Xilinx. The Block RAM column in Table I indicates the number of 18kb BRAM blocks needed on the FPGA. It can be seen that resource utilization increases proportionally with the number of sub-filters. For 64 sub-filters, 64% of the slice LUTs (lookup tables) are used, and a maximum of approximately 90 sub-filters can fit onto a single Artix-7 (xc7a200tfg484-1) FPGA platform.

B. Execution time

The proposed design utilizes K parallel sub-filters, thus bringing down the number of particles processed within a sub-filter to N/K . Since sampling and importance blocks are pipelined, these steps take $N/K + \tau_s + \tau_i$ clock cycles and the re-sampling step takes $3N/K + \tau_r$ cycles to process N/K particles, where τ_s , τ_i and τ_r represent the start-up latency of the sampling, importance and re-sampling units, respectively. Since all the K sub-filters are parallelized, the time taken to process a total of N particles for the SIR operation is:

$$T_{SIR} = (4N/K + \tau)T_{clk}$$

where, $\tau = \tau_s + \tau_i + \tau_r$ and T_{clk} is the clock period of the design.

Fig. 8 gives the timing diagram for completion of SIR operations using the proposed architecture for N particles, for a single iteration. Furthermore, since particle routing is incorporated within the sampling step, the transfer of particles between the sub-filters does not take any additional cycles. This makes the design scalable for a large number of sub-filters, as the routing operation requires no extra time.

In Fig. 9(a), we show the execution time of the proposed architecture as a function of the number of sub-filters (K) for different N . As expected, the execution time increases with the number of particles (N). In many applications, for example, in biomedical signal processing, the state space dimension is

very high [22]. Consequently, large number of particles are needed to achieve satisfactory performance. In such cases, the computation time often becomes unrealistic. Introducing parallelization in the design by using more sub-filters (K) brings down the execution time significantly, as shown in Fig. 9(a). The latency used for the plot is $\tau = 50$ cycles. However, the reduction in execution time by increasing K comes at the cost of added hardware, which can be inferred from Fig. 9(b). Thus, there is a trade-off between the speed and the hardware utilized. For instance, using a single sub-filter, and no parallelization uses a mere 1.4k (1%) LUTs to process 256 particles, and the time taken for SIR operations is around 1075 clock cycles. On the other hand, with a design consisting 8 sub-filters, it takes only 178 clock cycles for SIR operations, but utilizes 11k (8%) LUTs. Thus, there is a trade-off between speed and hardware used. The given FPGA resources limit the total number of sub-filters that can be accommodated on an FPGA, thus limiting the maximum achievable speed.

C. Estimation accuracy

We analyzed the estimation accuracy for the 2D source localization problem as a function of the number of particles (N) for the standard and modified SIR algorithms. The estimation error gives the error between the actual source location and the estimated source location given by:

$$Error = \sqrt{(pos_x - x)^2 + (pos_y - y)^2} \quad (14)$$

where, pos_x and pos_y denote the estimated position of the source obtained from the PF algorithm, in 2D Cartesian coordinate system. x and y denote the true position of the source in the 2D arena.

The algorithm for the standard SIR filter is presented in Section. III and has no parallelization incorporated. The modified SIR algorithm implements parallelization by utilizing K sub-filters working concurrently to reduce the execution time and is introduced in Section. V. The estimation errors presented in Fig. 9(c) are the average errors in 1000 runs over 250 time-steps. It is inferred that there is no significant difference in the estimation error between the standard and the modified SIR algorithm. Additionally, the modified algorithm achieves lower execution time and allows the parallel computation of

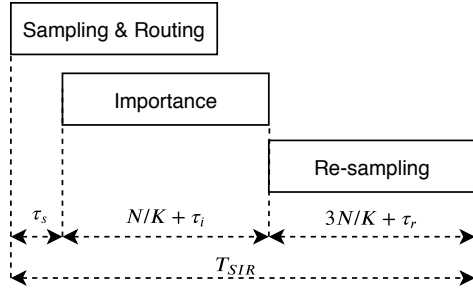


Fig. 8: Timing diagram for SIR operations of the proposed design.

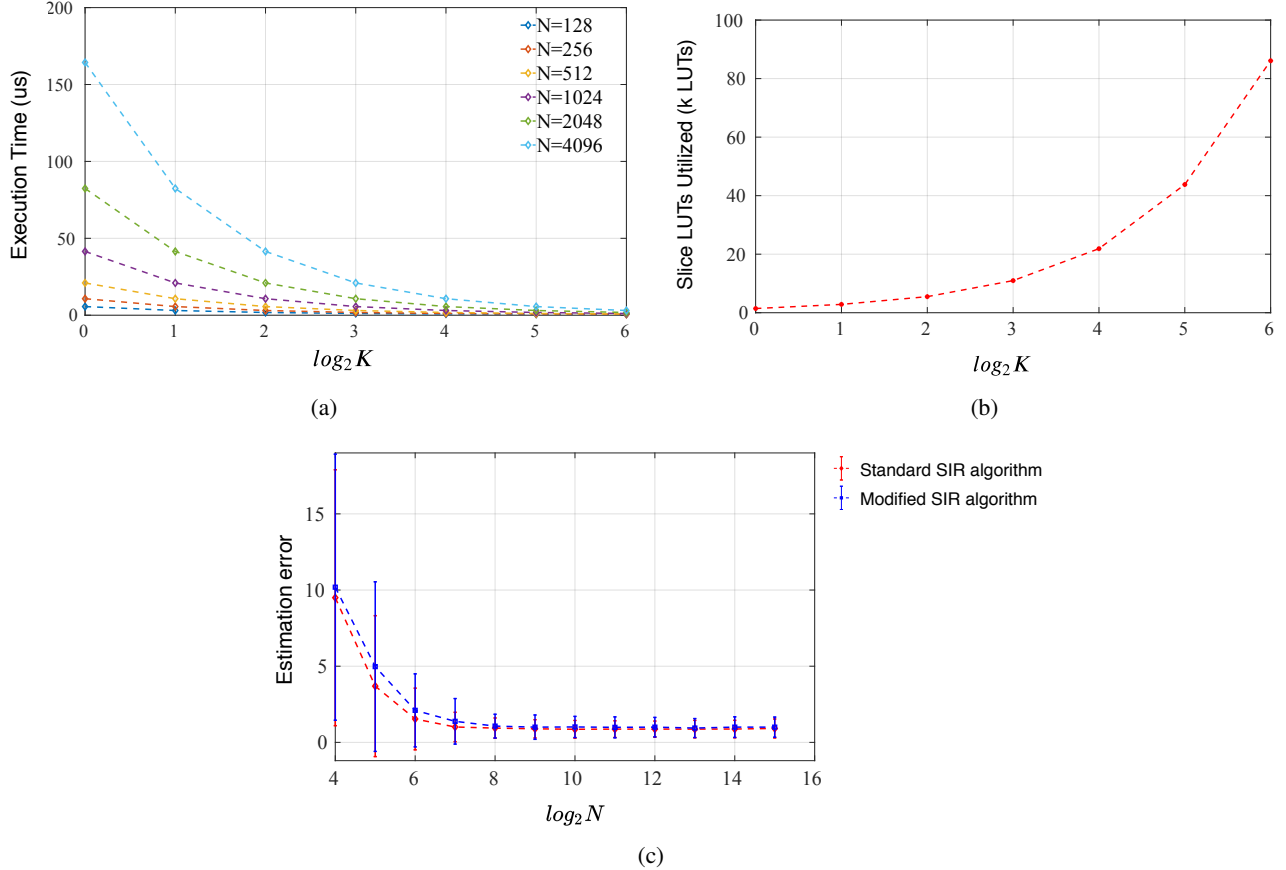


Fig. 9: Performance analysis of the proposed design. (a) Execution time of the proposed design as a function of the number of sub-filters (K), for different number of particles (N). (b) Resource utilization in terms of the number of slice LUTs used as a function of the number of sub-filters (K). (c) Estimation error as a function of the number of particles (N) for the standard SIR filter without any parallelization using Algorithm 1 and the modified SIR filter with parallelization using Algorithm 2.

PFs. Further, it is noted that by scaling the number of particles, the estimation accuracy improves as the error decreases.

D. Choice of number of sub-filters K

Choice of the number of sub-filters (K) used in the design depends on several factors, such as the number of particles (N), the clock frequency of the design (f_{clk}), and the observation sampling rate (f_s) of the measurement samples. The sampling rate gives the rate at which new input measurements can be processed. N is chosen depending on the application for which the particle filter is applied. f_{clk} is selected based on the

maximum frequency supported by the design. The sampling rate is related to the execution time (T_{SIR}) of the filter as:

$$f_s = 1/T_{SIR} = \frac{f_{clk}}{(4N/K + \tau)}$$

where, $f_{clk} = 1/T_{clk}$. Thus, for a specified measurement sampling rate (f_s), clock frequency of the design (f_{clk}), and the number of particles (N), we can determine the number of sub-filters (K) needed from the above equation. For instance, in our application, we use 256 particles because the error curve levels off at $N = 256$ (cf. Fig. 9(c)), and there is no improvement in the estimation error by further increasing N .

Thus, to achieve a sampling rate of $f_s = 562$ kHz, with 256 particles and clock frequency $f_{clk} = 100$ Mhz, we utilize $K = 8$ sub-filters. The maximum number of sub-filters that can be used in the design depends on the resources of the given FPGA.

E. Comparison with state-of-the-art FPGA implementations

A comparison of our design with state-of-the-art FPGA implementation schemes is provided in Table II. To obtain a valid assessment with other works, we have used $N = 1,024$ particles (although 256 particles are sufficient for our application as error curve levels off at $N = 256$ (cf. Fig. 9(c)) and $K = 8$ sub-filters for the comparison. Most of the existing implementation schemes in literature implement the standard SIR algorithm (cf. Algorithm 1), which lacks parallelization. Moreover, their architectures are not scalable to process a large number of particles at a high sampling rate, as the execution time is proportional to the number of particles. Also, the re-sampling step is a major computational bottleneck, as it is inherently not parallelizable. In this work, we propose a modification to the existing algorithm that overcomes this computation bottleneck of the PF algorithm and makes the high-speed implementation possible. We introduce an additional particle routing step (cf. Algorithm 2) allowing for parallel re-sampling. We develop a PF architecture based on the modified algorithm incorporating parallelization and pipelining design strategies to reduce the execution time. Our design achieves very high input sampling rates, even for a large number of particles, by scaling the number of sub-filters K .

The first hardware architecture for implementing PFs on an FPGA was provided by Athalye et al. [8], applied to a tracking problem. Their architecture is generic and does not incorporate any parallelization in the design. Thus, their architecture suffers from a low sampling rate of about 16 kHz for 2048 particles, which is approximately 11 times lower than the sampling rate of our design. However, owing to the non-parallel architecture, the resource consumption of their design (4.3k registers and 3.8k LUTs) is relatively low. Another state-of-the-art system was presented in [12]. The authors implemented an SIR filter on the Xilinx Virtex-5 FPGA platform for bearings-only tracking application and achieved a sampling rate of 46 kHz for 1024 particles. Regarding its hardware utilization, it uses 13.6k registers and 7.3k LUTs, which are comparable to those of our design; however, their sampling rate is four times lower than that of our system. Sileshi et al. [13] proposed two methods for implementing PFs on hardware. The first method was a hardware/software (HW/SW) co-design approach, where the software components were implemented using an embedded processor (MicroBlaze). The hardware part was based on a PF hardware acceleration module on an FPGA. This HW/SW co-design approach has a low sampling rate of about 1 kHz due to communication overhead between the MicroBlaze soft processor and the hardware acceleration module. Further, speedup of the design by utilizing a large number of parallel particle processors is limited by the number of bus interfaces available

in the soft-core processor (MicroBlaze). Thus, to improve the sampling rate, they proposed a second approach which is entirely a hardware design. However, their architecture does not support parallel processing and achieves a low sampling rate of about 18 kHz, whereas our system can sample at 178 kHz for processing the same 1024 particles. Their full hardware system utilizes 1.4k registers and 19k LUTs. Velmurugan [16] proposed a fully digital PF FPGA implementation for tracking application, without any parallelization in the design. They used a high-level Xilinx system generator tool to generate the VHDL code for deployment on a Xilinx FPGA from Simulink models or MATLAB code. Their design is not optimized in terms of hardware utilization as they use a high-level abstraction tool and lack flexibility to fine-tune the design. On the other hand, our design is completely hand-coded in Verilog and provides granular control to tweak the design parameters and provides flexibility for easy integration of the design in numerous PF applications. They achieve a sampling rate of about 30 kHz for 1000 particles, which is six times lower than that of our design. Further, their resource consumption is relatively high (17.4k registers and 30.9k LUTs) as they use high-level abstraction tools for implementation.

Our system has a comparable resource utilization (12.3k registers and 10.9k LUTs for 8 sub-filters) with a low execution time of about $5.62 \mu s$ and can achieve a very high input sampling rate of about 178 kHz compared to other designs. Our design can be used in real-time applications due to the low execution time. Further, to achieve a high sampling rate even with a large number of particles, more sub-filters can be used, as shown in Fig. 9(a). However, this comes at the cost of added hardware. On the other hand, the resource utilization of our system can go as low as 1.7k registers and 1.4k LUTs using a single sub-filter (cf. Table I) for applications that have stringent resource constraints, but at the cost of increased execution time (cf. Fig. 9(a)).

F. Experimental results

The experimental result for the 2-dimensional source localization is shown in Fig. 10. State in this 2D model is 2-dimensional and incorporates position in x and y directions. The input to the design is binary measurements from a set of 8 photodiodes and the instantaneous position of the UGV. The inputs are sampled and processed by the PF system over 250 time-steps on an FPGA to estimate the source location. We consider the probabilities α and β to be 0.8 and 0.6, respectively. It can be seen that the algorithm is robust enough to localize the source even with a noise probability of 0.6. However, with an increase in noise probability (β), the number of time-steps or iterations required to localize the source also increases, as shown in Fig. 11. The source is considered to be localized if the estimation error is less than the predetermined threshold, which is 2.5 in our case. The time-steps shown in Fig. 11 are the average time required to localize the source over 500 runs. The entire design was coded in Verilog HDL, and the design was implemented on an FPGA.

We converted all variables from a floating-point to a fixed point representation for the implementation on an FPGA. We

TABLE II: Performance summary and comparison with state-of-the-art particle filter FPGA implementation schemes.

Reference	Athalye et al. [8]	Ye and Zhang [12]	Sileshi et al. [13]	Velmurugan [16]	This Work
Application	Tracking	Tracking	Localization	Tracking	Localization
FPGA Device	Xilinx Virtex II pro	Xilinx Virtex-5	Xilinx Kintex-7	Xilinx Virtex II pro	Xilinx Artix-7
Number of particles (N)	2,048	1,024	1,024	1,000	1,024
Slice Registers	4,392	13,692	1,462	17,418	12,356
Slice LUTs	3,848	7,379	19,116	30,900	10,973
Clock Frequency	100 MHz	100 MHz	100 MHz	100 MHz	100 MHz
Execution Time (μ s)	60.24	21.74	55.37	33.33	5.62*
Sampling Rate (kHz)	16	46	18	30	178*

* $K = 8$ sub-filters are used for the calculation.

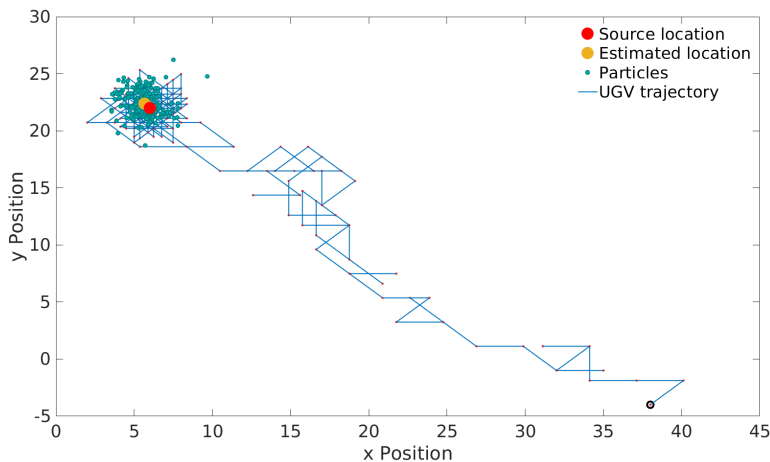


Fig. 10: 2D source localization experimental result. The source is positioned at $[6, 22]$ marked by a 'red' circular dot. At the start, the UGV is positioned at $[38, -4]$. The model is run over 250 time-steps for 256 particles, and the UGV traverses towards the source based on sensor measurements. The final source estimate (pos_t) obtained by the PF algorithm is marked by a 'yellow' circular dot and has an estimation error of 0.5.

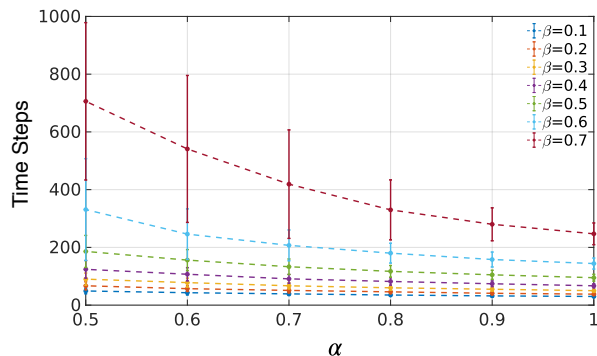


Fig. 11: Variation in the number of time-steps required to localize the source as a function of α and β .

have used a 16-bit fixed-point representation for particles and their associated weights. All bearing-related information, such as the angle of the UGV and the angle of particles used in the importance block, is represented by a 12-bit fixed-point representation. Further, the indices of the replicated and the discarded particles are integers and are represented using $\log_2(M) = 5$ bits. The output estimate of the source location (pos_t) is represented using a 16-bit representation. $N = 256$ particles were used for processing. $K = 8$ sub-filters were used in the design with $M = 32$ particles processed within each sub-filter. $M/2 = 16$ particles were exchanged between

the sub-filters after the completion of every iteration as a part of particle routing operation. The time taken to complete SIR operations for $N = 256$ and $K = 8$ is 178 clock cycles. Using a clock frequency of 100 MHz, the speed at which we can process new samples is around 562 kHz, and the execution time for SIR operation is 1.78μ s. This high sampling rate enables us to use the proposed hardware architecture in various real-time applications.

Further, we show that the 2D source localization problem can be extended to 3D, and we have modelled it in software using MATLAB. This 3D model incorporates position along

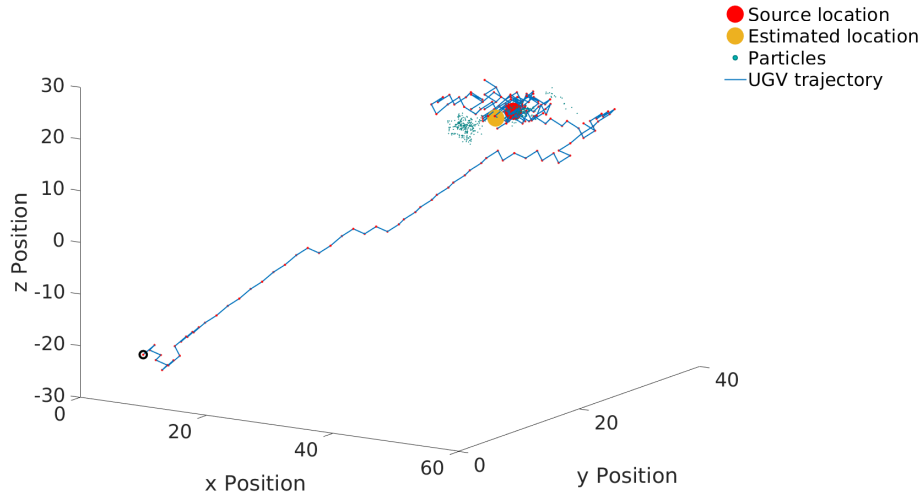


Fig. 12: 3D source localization experimental result. The source is positioned at $[40, 30, 20]$, and the initial position of the UGV is $[10, 0, -20]$. The model runs over 350 time-steps for 512 particles. Here, the UAV traverses in three dimensions to move towards the source. The error between the source and the estimated location is 2.2.

the x , y , and z directions. Here, an Unmanned Aerial Vehicle (UAV) can be utilized to localize the source. As compared to 8 sensors used in 2D localization, here we utilize 16 sensors for scanning the entire 3D space. We consider $\alpha = 0.8$ and $\beta = 0.4$, and the model was run over 350 time-steps for 512 particles to localize the source. The result is presented in Fig. 12. The estimation error between the actual source location and the estimated source location in the 3D arena is given by:

$$Error = \sqrt{(pos_x - x)^2 + (pos_y - y)^2 + (pos_z - z)^2} \quad (15)$$

where, pos_x , pos_y and pos_z denote the estimated position of the source obtained from PF algorithm, in 3D Cartesian coordinate system. x , y and z represent the true position of the source in 3D arena.

VIII. CONCLUSIONS AND OUTLOOK

In this paper, we presented an architecture for hardware realization of PFs, particularly sampling, importance, and re-sampling filters, on an FPGA. PFs perform better than traditional Kalman filters in non-linear and non-Gaussian settings. Interesting insights into the advantages of PFs, performance comparison, and trade-offs of PFs over other non-PF solutions are provided by [28], [29]. However, PFs are computationally very demanding and take a significant amount of time to process a large number of particles; hence, PFs are seldom used for real-time applications. In our architecture, we try to address this issue by exploiting parallelization and pipelining design techniques to reduce the overall execution time, thus making the real-time implementation of PFs feasible. However, a major bottleneck in high-speed parallel implementation of the SIR filter is the re-sampling step, as it is inherently not parallelizable and cannot be pipelined with other operations. In this regard, we modified the standard SIR filter to make it parallelizable. The modified algorithm has an additional

particle routing step and utilizes several sub-filters working concurrently and performing SIR operations independently on particles to reduce the overall execution time. The architecture presented is massively parallel and scalable to process a large number of particles and has low design complexity.

A performance assessment in terms of the resources utilized on an FPGA, execution time, and estimation accuracy is presented. We also compared the estimation error of the modified SIR algorithm with that of the standard SIR algorithm and noted that there is no significant difference in the estimation error. The proposed architecture has a total execution time of about $5.62 \mu s$ (i.e., a sampling rate of 178 kHz) by utilizing 8 sub-filters for processing $N = 1024$ particles. We compared our design with state-of-the-art FPGA implementation schemes and found that our design outperforms other implementation schemes in terms of execution time. The low execution time (i.e., high input sampling rate) makes our architecture ideal for real-time applications.

The proposed PF architecture is not limited to a particular application and can be used for other applications by modifying the importance block of the sub-filter. The sampling and re-sampling block designs are generic and can be used for any application. In this work, we validated our PF architecture for the source localization problem to estimate the position of a source based on received sensor measurements. Our PF implementation is robust to noise and can predict the source position even with a high noise probability. Experimental results show the estimated source location with respect to the actual location for 2D and 3D settings and demonstrate the effectiveness of the proposed algorithm.

In recent times, there has been an increase in the utilization of UGVs in several instances, such as disaster relief and military applications, due to reduced human involvement and the ability to carry out the task remotely. The proposed source localization framework using PFs can autonomously navigate

and localize the source of interest without any human intervention, which would be very helpful in missions wherein there is an imminent threat involved, such as locating chemical, biological or radiative sources in an unknown environment. Further, the proposed PF framework and its hardware realization would be useful for the signal processing community for solving various state estimation problems such as tracking, navigation, and positioning in real-time.

REFERENCES

- [1] A. Farina, "Target tracking with bearings only measurements," *Signal Processing*, vol. 78, no. 1, pp. 61 – 78, 1999. [Online]. Available: <http://www.sciencedirect.com/science/article/pii/S016516849900047X>
- [2] N. J. Gordon, D. J. Salmond, and A. F. M. Smith, "Novel approach to nonlinear/non-Gaussian Bayesian state estimation," *IEEE Proceedings F - Radar and Signal Processing*, vol. 140, no. 2, pp. 107–113, Apr. 1993.
- [3] M. Tian, Y. Bo, Z. Chen, P. Wu, and C. Yue, "Multi-target tracking method based on improved firefly algorithm optimized particle filter," *Neurocomputing*, vol. 359, pp. 438 – 448, 2019. [Online]. Available: <http://www.sciencedirect.com/science/article/pii/S09252321219308240>
- [4] N. Merlinge, K. Dahia, and H. Piet-Lahanier, "A Box Regularized Particle Filter for terrain navigation with highly non-linear measurements," *IFAC-Papers*, vol. 49, no. 17, pp. 361 – 366, 2016.
- [5] Z. Zhang and J. Chen, "Fault detection and diagnosis based on particle filters combined with interactive multiple-model estimation in dynamic process systems," *ISA Transactions*, vol. 85, pp. 247 – 261, 2019. [Online]. Available: <http://www.sciencedirect.com/science/article/pii/S001905781830394X>
- [6] A. Doucet, S. Godsill, and C. Andrieu, "On sequential Monte Carlo sampling methods for Bayesian filtering," *Statistics and Computing*, vol. 10, no. 3, pp. 197–208, July 2000. [Online]. Available: <https://doi.org/10.1023/A:1008935410038>
- [7] M. S. Arulampalam, S. Maskell, N. Gordon, and T. Clapp, "A tutorial on particle filters for online nonlinear/non-Gaussian Bayesian tracking," *IEEE Transactions on Signal Processing*, vol. 50, no. 2, pp. 174–188, Feb. 2002.
- [8] A. Athalye, M. Bolić, S. Hong, and P. M. Djurić, "Generic hardware architectures for sampling and resampling in particle filters," *EURASIP Journal on Advances in Signal Processing*, vol. 2005, no. 17, p. 476167, Oct. 2005. [Online]. Available: <https://doi.org/10.1155/ASP.2005.2888>
- [9] M. Bolić, P. M. Djurić, and S. Hong, "Resampling algorithms and architectures for distributed particle filters," *IEEE Transactions on Signal Processing*, vol. 53, no. 7, pp. 2442–2450, July 2005.
- [10] L. Miao, J. J. Zhang, C. Chakrabarti, and A. Papandreou-Suppappola, "Algorithm and parallel implementation of particle filtering and its use in waveform-agile sensing," *Journal of Signal Processing Systems*, vol. 65, no. 2, p. 211, July 2011. [Online]. Available: <https://doi.org/10.1007/s11265-011-0601-2>
- [11] S. Agrawal, P. Engineer, R. Velmurugan, and S. Patkar, "FPGA implementation of particle filter based object tracking in video," in *2012 International Symposium on Electronic System Design (ISED)*, Dec. 2012, pp. 82–86.
- [12] B. Ye and Y. Zhang, "Improved FPGA implementation of particle filter for radar tracking applications," in *2009 2nd Asian-Pacific Conference on Synthetic Aperture Radar*, 2009, pp. 943–946.
- [13] B. G. Sileshi, J. Oliver, and C. Ferrer, "Accelerating particle filter on FPGA," in *2016 IEEE Computer Society Annual Symposium on VLSI (ISVLSI)*, July 2016, pp. 591–594.
- [14] B. Sileshi, C. Ferrer, and J. Oliver, "Chapter 2 - Accelerating Techniques for Particle Filter Implementations on FPGA," in *Emerging Trends in Computational Biology, Bioinformatics, and Systems Biology*, 2015, pp. 19 – 37. [Online]. Available: <http://www.sciencedirect.com/science/article/pii/B9780128025086000028>
- [15] B. Sileshi, J. Oliver, R. Toledo, J. Gonçalves, and P. Costa, "On the behaviour of low cost laser scanners in HW/SW particle filter SLAM applications," *Robotics and Autonomous Systems*, vol. 80, pp. 11 – 23, 2016. [Online]. Available: <http://www.sciencedirect.com/science/article/pii/S0921889015303201>
- [16] R. Velmurugan, "Implementation strategies for particle filter based target tracking," *Ph.D thesis, School of Electrical and Computer Engineering, Georgia Institute of Technology*, May 2007.
- [17] G. Hendeby, J. D. Hol, R. Karlsson, and F. Gustafsson, "A graphics processing unit implementation of the particle filter," in *2007 15th European Signal Processing Conference*, Sep. 2007, pp. 1639–1643.
- [18] L. M. Murray, A. Lee, and P. E. Jacob, "Parallel resampling in the particle filter," *Journal of Computational and Graphical Statistics*, vol. 25, no. 3, pp. 789–805, 2016. [Online]. Available: <https://doi.org/10.1080/10618600.2015.1062015>
- [19] M. Bolić, A. Athalye, P. M. Djurić, and S. Hong, "Algorithmic modification of Particle Filters for hardware implementation," in *2004 12th European Signal Processing Conference*, Sep. 2004, pp. 1641–1644.
- [20] M. Chitchian, A. Simonetto, A. S. van Amesfoort, and T. Keviczky, "Distributed computation particle filters on GPU architectures for real-time control applications," *IEEE Transactions on Control Systems Technology*, vol. 21, no. 6, pp. 2224–2238, Nov. 2013.
- [21] Y. Q. Zhang, T. Sathyan, M. Hedley, P. H. W. Leong, and A. Pasha, "Hardware efficient parallel particle filter for tracking in wireless networks," in *2012 IEEE 23rd International Symposium on Personal, Indoor and Mobile Radio Communications - (PIMRC)*, Sept. 2012, pp. 1734–1739.
- [22] L. Miao, J. J. Zhang, C. Chakrabarti, and A. Papandreou-Suppappola, "Multiple sensor sequential tracking of neural activity: Algorithm and FPGA implementation," in *2010 Conference Record of the Forty Fourth Asilomar Conference on Signals, Systems and Computers*, 2010, pp. 369–373.
- [23] C. S. Thakur, S. Afshar, R. M. Wang, T. J. Hamilton, J. Tapson, and A. van Schaik, "Bayesian Estimation and Inference Using Stochastic Electronics," *Frontiers in Neuroscience*, vol. 10, p. 104, 2016. [Online]. Available: <https://www.frontiersin.org/article/10.3389/fnins.2016.00104>
- [24] J. L. Palmer, R. Cannizzaro, B. Ristic, T. Cheah, C. V. D. Nagahawatte, J. L. Gilbert, and S. Arulampalam, "Source localisation with a Bernoulli particle-filter-based bearings-only tracking algorithm," 2015.
- [25] E. Milovanović, M. Stojcev, I. Milovanović, T. Nikolic, and Z. Stamenkovic, "Concurrent generation of pseudo random numbers with LFSR of Fibonacci and Galois type," *Computing and Informatics*, vol. 34, Aug. 2015.
- [26] "CORDIC v6.0 LogiCORE IP Product Guide," *Xilinx, Product Guide*, pp. 1–66, 2017.
- [27] "Block Memory Generator v8.4," *Xilinx, LogiCORE IP Product Guide*, pp. 1–129, 2017.
- [28] F. Ababsa, M. Malle, and D. Roussel, "Comparison between particle filter approach and Kalman filter-based technique for head tracking in augmented reality systems," in *IEEE International Conference on Robotics and Automation, 2004. Proceedings. ICRA '04. 2004*, vol. 1, 2004, pp. 1021–1026.
- [29] N. Y. Ko and T. G. Kim, "Comparison of Kalman filter and particle filter used for localization of an underwater vehicle," in *2012 9th International Conference on Ubiquitous Robots and Ambient Intelligence (URAI)*, 2012, pp. 350–352.